Enhanced catalytic degradation of 4-NP using a superhydrophilic PVDF membrane decorated with Au nanoparticles

Ziyang Wu,[ab] Haibo Lin,[a] Yunze Wang,[a] Xuemin Yu,[ab] Jinglong Li,[a] Zhu Xiong,[a] Yi Wang,[a] Youju Huang,[a] Tao Chen[a] and Fu Liu*[a]

Poly(vinylidene fluoride) (PVDF) membranes have been widely applied to treat wastewater, however, the removal of toxic aromatic phenolic compounds remains a technical challenge due to the serious adsorption fouling and difficult degradation. Herein, we aimed to design a superhydrophilic PVDF membrane decorated with Au nanoparticles, which enhanced the rapid degradation of *p*-nitrophenol (4-NP). The superhydrophilic PVDF membrane with a micro/nano structured surface was decorated with Au nanoparticles *via* poly(dopamine) (PDA) as a spacer. The influences of membrane affinity (*e.g.* Hydrophilic Membrane (HM), micro/nano structured superhydrophilic membrane (MSiM), and micro/nano structured superhydrophobic membrane (MSoM)) on PDA deposition and the subsequent Au decoration were comprehensively investigated. The synthesized Au nanoparticles were characterized using transmission electron microscopy (TEM) and UV-vis absorption spectra. The morphology and composition was evaluated using scanning electron microscopy (SEM) and X-ray photoelectron spectroscopy (XPS). Static catalytic experiments demonstrated that MSiM degraded over 90% of 4-NP in 5 minutes with a kinetic reaction rate constant of 47.84×10^{-2} min^{-1} and high stability over 6 cycles. A membrane catalytic reactor (MCR) was designed to realize the continuous catalytic degradation of 4-NP with a kinetic reaction rate constant of 7×10^{-2} min^{-1}.

1. Introduction

In recent years, nanocomposite materials have expanded markedly in membrane separation areas. Nano particles such as Al_2O_3,[1] SiO_2,[2] Fe_3O_4,[3] ZrO_2,[4] and TiO_2 (ref. 5) have been widely used to fabricate nanocomposite polymeric membranes due to their hydrophilicity and large surface area-to-volume ratio.[6] The porous polymeric membrane prevails in highly efficient separation in wastewater treatment, however, the separation performances are easily compromised by the fouling of proteins or organic-molecules. Highly toxic aromatic organic compounds *e.g. p*-nitrophenol are difficult to treat through traditional biodegradation. The reduction of *p*-nitrophenol to *p*-aminophenol *via* nano-catalysts provides an efficient solution. However, in heterogeneous catalytic cases, the catalytic nanoparticles cannot be well dispersed in the solution, and also the recycling of the used catalysts is difficult due to the inevitable loss, which causes post energy and cost burden. The idea of integrating membrane separation with nanoparticle catalysis is most likely to overcome the above deficiencies. A membrane catalytic reactor (MCR) is capable of degrading the toxic micro-pollutants and reducing the membrane fouling. Besides, the long term catalytic stability can be maintained *via* embedding nano-catalysts firmly on the porous membranes.

Damodar *et al.* prepared a self-cleaning and antibacterial PVDF membrane by incorporating different amounts of photocatalytic TiO_2 (0–4 wt%).[7] Compared to the neat PVDF membrane, the TiO_2 entrapped PVDF membrane showed a better antibacterial ability under UV. However, the catalytic removal of RB5 is not as good as expected. Dotzauer *et al.* succeeded in the preparation of coating polyelectrolyte/Au nanoparticles on porous alumina membranes by a layer-by-layer adsorption method.[8] The modified alumina membranes reduced >99% of 0.4 mM 4-nitrophenol at a linear flow rate of 0.98 cm s^{-1}. An antibacterial membrane can be prepared by dipping the membrane in dopamine and silver nitrate solution alternatively.[9] Besides, multilayer multi-metal nanoparticles can be generated by repeating the dipping procedure in dopamine and metallic ion solution (*e.g.* Ag or Au), which demonstrated both enhanced antibacterial effects and catalytic degradation for methylene blue.

The previous research on the incorporation of nanoparticles into polymeric membranes are mainly to enhance the hydrophilicity, fouling resistance or antibacterial performance. It is likewise of interest for producing a catalytic PVDF membrane for the degradation of toxic micro-pollutants *e.g.* aromatic

[a]*Ningbo Institute of Materials Technology & Engineering, Chinese Academy of Sciences, Ningbo, 315201, P. R. China. E-mail: fu.liu@nimte.ac.cn; Tel: +86-574-863259636*
[b]*University of Chinese Academy of Sciences, Beijing, 100049, P. R. China*

compound *p*-nitrophenol. PVDF was chosen as the substrate membrane due to its good chemical resistance, thermal stability and mechanical properties.[10–12] And the new composite functional material such as the carbon nanotube/poly(vinylidene fluoride) which can increase the dielectric constant at very low volume fractions was commendably researched as well.[13–15] *p*-Nitrophenol was chosen as the target molecule due to its difficult biodegradation and high toxicity as a model of organic aromatic compounds. Poly(dopamine) (PDA) has drawn tremendous interest recently as an universal surface modification agent in wide applications of biotechnology,[16–18] electrochemical,[19,20] nanotechnology,[21,22] and membrane[23,24] applications. Typically, dopamine can be self-oxidized to produce an adhesive PDA layer on various material surfaces in alkaline environments (*e.g.* 10 mM Tris, pH 8.5).[25] The PDA layer provides reactive –OH groups, which consequently anchor the nanoparticles onto the substrate surface.[26] The mechanism of the possible self-oxidation process of dopamine is suggested in Fig. 1.

Illuminated by the previous studies, we designed a feasible strategy to load Au nanoparticles (AuNPs) on a porous PVDF membrane using dopamine as a super bio-glue. Both the micro/nano-morphology and the affinity of the porous PVDF membrane are crucial to the deposition of PDA and subsequent decoration with AuNPs. In our previous work, we fabricated a superhydrophilic–superoleophilic membrane with a micro/nano textured surface *via* a template methodology, which showed excellent oil/water separation performance.[27] The specially designed micro/nano surface will possibly promote the adsorption of PDA and Au nanoparticles thanks to the high specific area and the high hydrophilicity. Herein, we aim to design a membrane catalytic reactor (MCR) to realize the high efficient static and dynamic degradation of *p*-nitrophenol. The synthesis route of the catalytic PVDF membrane is illustrated in Fig. 2. PVDF membranes with different affinities were first prepared by phase separation.[28,29] The prepared membranes were deposited by the PDA layer *via* self-oxidation. Finally,

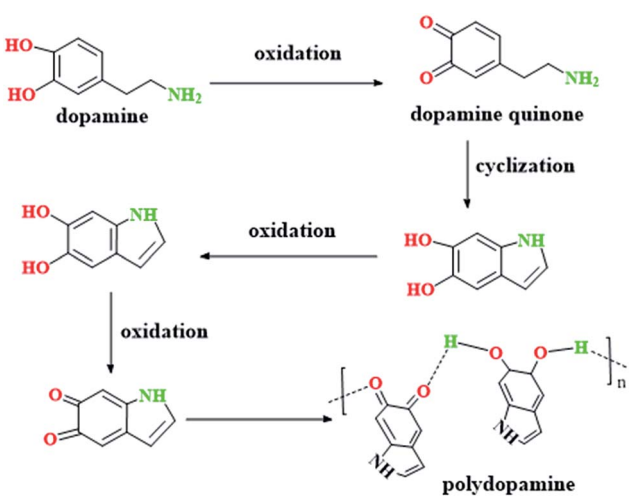

Fig. 1 The mechanism of the dopamine self-oxidation process.

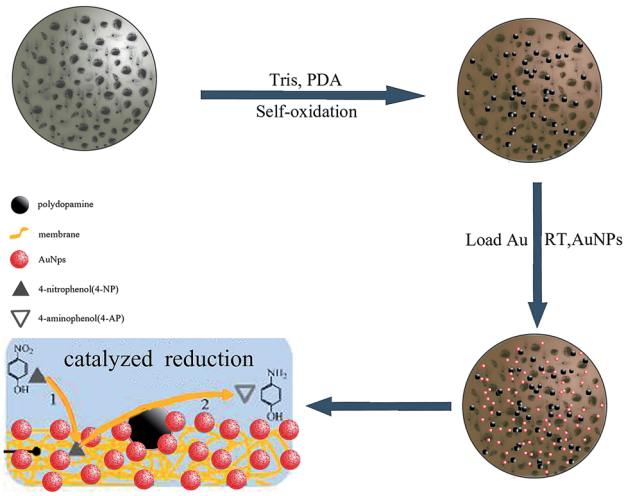

Fig. 2 The synthesis route of the catalytic PVDF membrane decorated with AuNPs *via* PDA as a spacer.

AuNPs were anchored onto the membrane using *in situ* embedding.

2. Experimental section

2.1 Materials

PVDF (Kynar 761A, Arkema) dried at 80 °C for 24 h was used to prepare the membrane. Triethyl phosphate (TEP), vinyltriethoxysilane (VTES, 98 wt%), and sodium borohydride ($NaBH_4$, 98 wt%) were purchased from Sinopharm Chemical reagent Co. Dopamine hydrochloride (98 wt%, Aldrich), tris(hydroxymethyl)aminomethane (Tris, 99.9 wt%, Aldrich), $HAuCl_4 \cdot xH_2O$ (Au 47.8 wt%), 2,2′-azobis(2-methyl propionitrile) (AIBN, 99%, Aladdin), *p*-nitrophenol (4-NP, 98 wt%, Aldrich) and deionized water were all directly used without further purification.

2.2 Synthesis of AuNPs

All glassware was thoroughly cleaned in aqua regia (3 parts HCl, 1 part HNO_3), rinsed in triply distilled H_2O, and oven-dried prior to use. Au NPs were synthesized using sodium citrate reduction of $HAuCl_4$ in deionized water. Au colloids were prepared according to Frens[30] or Sutherland[31] with slight modifications.

Typically, 90 mL of deionized water was brought to a rolling boil (120 °C) with vigorous stirring (800 rpm) which was continued for 10 min. 10 mL of sodium citrate was added to the solution in one minute, which resulted in a color change from pale yellow to wine red in 10 minutes after adding 10 mL of 2.5 M $HAuCl_4$ to the vortex of the solution. The solution was under continuous stirring at 120 °C for 20 minutes.

2.3 Preparation of the PVDF membranes with different affinities

The hydrophilicity of PVDF membranes will influence the deposition of PDA and the decoration with AuNPs. Therefore,

PVDF membranes with different affinities (hydrophilic membrane (HM), micro/nano structured superhydrophilic membrane (MSiM), and micro/nano structured superhydrophobic membrane (MSoM)) were produced respectively as follows:

HM and MSiM are both prepared using an interfacial crosslinking strategy. A hydrophilic precopolymer solution was first synthesized: 0.08 g of AIBN, 3.75 g of NVP and 2.75 g of VTES were dissolved in 1100 g of TEP. The solution was vigorously stirred under a nitrogen atmosphere for 1 hour at room temperature to remove the oxygen. Then the temperature was upgraded to 80 °C for 24 h with vigorous stirring to obtain the final hydrophilic precopolymer P(VP-VTES) solution.

For the fabrication of HM and MSiM: 15 g of PVDF in 85 g of triethyl phosphate (TEP) was totally dissolved at 80 °C. The reaction was carried out at 80 °C with vigorous stirring for 24 h. Afterwards, the PVDF solution was spread onto a clean glass plate or non-woven fabric (NWF) (70 g m^{-2}) using a casting knife with a thickness of 300 μm. The nascent membrane was immediately immersed into a 25 °C coagulation bath composed of a TEP/water mixture (v/v: 1/1) for 5 s, and moved to a pure water bath for total solidification. The membrane was transferred to 25 °C fresh deionized water for 24 h, and dried in the air for 24 h to get the nascent membrane. Finally, the membrane peeled from the glass plate was immersed in the above synthesized hydrophilic precopolymer P(VP-VTES) solution for 1 h at room temperature for the hydrolysis, condensation and interfacial crosslinking to obtain HM. Similarly, the membrane with the non-woven fabric (NWF) was first dipped in the above synthesized hydrophilic precopolymer P(VP-VTES) solution for 1 h at room temperature and then transferred into the citric acid solution (1 wt%) for 24 h to boost the interfacial crosslinking. The resultant membrane was dried and peeled off from the NWF to obtain the MSiM.

For the fabrication of the MSoM, 15 g of PVDF in 85 g of triethyl phosphate (TEP) was totally dissolved at 80 °C. The solution was carried out at 80 °C with vigorous stirring for 24 h. Afterwards, the PVDF solution was spread onto a non-woven fabric NWF (70 g m^{-2}) using a casting knife with a thickness of 300 μm. The pristine membrane was immediately immersed into a 25 °C coagulation bath composed of a TEP/water mixture (v/v: 1/1) for 5 s, and then moved to a pure water bath for total solidification. The resultant membrane was dried and peeled from the NWF to obtain the MSoM.

2.4 Preparation of the Au–PDA–PVDF membranes

0.2 g of dopamine was dissolved in 100 mL of Tris buffer (pH = 8.5), the hydrophilic PVDF membrane (HM) (A), the micro/nano structured superhydrophilic membrane (MSiM) (B), and the micro/nano structured superhydrophobic membrane (MSoM) (C) prepared above were immersed into the dopamine solution for 2, 8 and 24 h at room temperature to embed a PDA layer on the surface of the PVDF membrane (A_2, A_8, A_{24}, B_2, B_8, B_{24}, C_2, C_8, C_{24}). Subsequently, the PDA-coated samples were thoroughly washed with deionized (DI) water and immersed in 50 mL of the Au colloidal solution for 24 h at room temperature to obtain the catalytic Au–PDA–PVDF membrane ($A_{2\text{-}Au}$, $A_{8\text{-}Au}$, $A_{24\text{-}Au}$, $B_{2\text{-}Au}$, $B_{8\text{-}Au}$, $B_{24\text{-}Au}$, $C_{2\text{-}Au}$, $C_{8\text{-}Au}$, $C_{24\text{-}Au}$). The details are shown in Table 1.

2.5 Characterization of the membranes

Surface morphologies of the PVDF membranes were observed using scanning electron microscopy (SEM, Hitachi S-4800, Japan). The membrane roughness was measured using laser scanning confocal microscopy (LSCM, Zeiss LSM 700, Germany). The contact angle variation with drop age was recorded using a water contact angle system (OCA20, Dataphysics, Germany). The membrane surface composition was determined using XPS analysis (AXIS UTLTRADLD, Japan), using Al-Kα as the radiation source.

2.6 Catalytic performance measurement

For the static catalytic performance, a modified membrane with an area of 0.6 × 0.7 cm^2 was immersed into 1.5 mL of aqueous 4-NP (2.72 × 10^{-5} M). Subsequently, the above solution was mixed with 1.5 mL of fresh $NaBH_4$ solution (0.048 M). The reaction was carried out at room temperature at a standstill. With the help of UV-vis spectroscopy (Lambda 950, US), we evaluated the catalytic performance of the membrane.

For the dynamic catalytic performance, a membrane catalytic reactor (MCR) was designed *via* a dead-end filtration mode. A peristaltic pump (BT300-1F, Longer Pump, China) was used to control the solution flowing rate 0.121 mL s^{-1} for continuous circulation at room temperature. The diameter of the membrane is 2.5 cm, and a mixed solution composed of 4-NP (7.5 mL, 2.72 × 10^{-5} M) and $NaBH_4$ (7.5 mL, 0.048 M) was used in the experiment.

3. Results and discussion

3.1 Catalytic properties of the AuNPs

As shown in Fig. 3, the average diameter of the AuNPs is ~40 nm from the TEM image. The catalytic activity of the AuNPs toward 4-NP reduction is convincingly confirmed by the UV spectra in Fig. 3. Usually, the UV-vis peak of pure 4-NP aqueous solution is at ~317 nm, however, this adsorption peak shifted to ~400 nm due to the formation of 4-nitrophenolate ions after the reducer $NaBH_4$ was added. With the addition of the AuNPs into the mixture, 4-NP was rapidly reduced to *p*-aminophenol (4-AP) in 60 s, which was verified by the complete disappearance of the pristine strong peak at ~400 nm and the appearance of new

Table 1 The catalytic Au–PDA–PVDF membranes prepared with different PDA deposition times

Method	HM	MSiM	MSoM
2 h (PDA)	A_2	B_2	C_2
Load (AuNPs)	$A_{2\text{-}Au}$	$B_{2\text{-}Au}$	$C_{2\text{-}Au}$
8 h (PDA)	A_8	B_8	C_8
Load (AuNPs)	$A_{8\text{-}Au}$	$B_{8\text{-}Au}$	$C_{8\text{-}Au}$
24 h (PDA)	A_{24}	B_{24}	C_{24}
Load (AuNPs)	$A_{24\text{-}Au}$	$B_{24\text{-}Au}$	$C_{24\text{-}Au}$

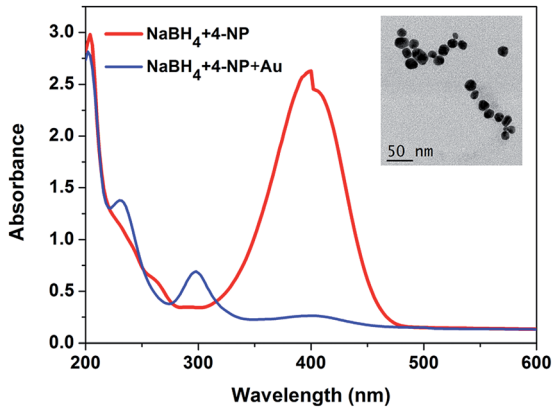

Fig. 3 TEM image and UV-visible spectra of 4-NP reduced using AuNP catalysis at 295 K, [4-NP] = 2.72 × 10^{-5} M, 1.5 mL, [$NaBH_4$] = 0.048 M, 1.5 mL, Au solution, 0.5 mL.

peaks at 230 nm and 300 nm.[32,33] However, the dispersed AuNPs in the solution are difficult to recycle and reuse due to the energy-consuming separation. Since the catalytic activity of Au is strongly dependant on the particle size, the reduction efficiency will be gradually retarded by the freely dispersed Au aggregation. To circumvent these distressing blocks, AuNPs were therefore integrated and anchored on porous membranes with different affinities. We will disclose the influences of the chemical affinity and physical texture on the dopamine deposition and AuNP immobilization.

3.2 Morphology and hydrophilicity of the PVDF membranes

The morphology and confocal roughness of the HM, MSiM and MSoM are shown in Fig. 4. The bottom surface of the HM with Rsa 1.905 nm was obviously flattened by the glass plate despite the presence of micropores. While for both the MSiM and MSoM, versatile textures are produced including microscaled petals, leaf-like structures and nanoscaled fibers by the NWF peeling. The roughness of the MSiM and MSoM is increased to 5.831 nm and 6.415 nm. The micro/nano texture was generated during the phase separation and well preserved by the flexible NWF template. The HM and MSiM were further modified using the interfacial crosslinking strategy to acquire better wettability. Specifically, PVP–VTES was firmly bonded on the rough membrane surface by the silane-based chemical crosslinking.

As shown in Fig. 5, the initial contact angle of the HM was 27.7°, and decreased rapidly to 0 in about 6 s, showing the good hydrophilicity. The MSiM showed instantaneous wettability with a prompt decay of contact angle from 19.1° to 0 in 2.5 s. The corresponding superhydrophilicity was mainly endowed by both the surface crosslinked PVP and micro/nano structure. In comparison, the MSoM demonstrated stable superhydrophobicity with a contact angle as high as 152.3° owing to the versatile texture and high roughness. The wettability influences the permeability despite the similar porous structure. The pure water flux of the HM, MSiM and MSoM is 7000 L m^{-2} h^{-1}, 8000 L m^{-2} h^{-1} and 80 L m^{-2} h^{-1} respectively. Both the physical texture and chemical affinity of the membrane are anticipated to affect PDA deposition and subsequent AuNP growth.

3.3 Morphology and chemistry of the Au–PDA–PVDF membranes

Mussel-inspired chemistry is a simple, universal, environmentally benign and multifunctional strategy to tune surface engineering. Dopamine has a high tendency to form a self-oxidation PDA coating on various polymeric substrates under alkaline conditions and air atmosphere. The PDA coating layer acts as a spacer for the post-modification. However, the deposition of dopamine is significantly influenced by surface chemistry, wettability and the microstructure due to the complex covalent and non-covalent interactions (including hydrogen bonding, π–π stacking and charge transfer interactions *etc.*). The varied morphological evolutions of the HM, MSiM and MSoM with different deposition times in dopamine solution for 2 h, 8 h and 24 h are shown in Fig. 6. It can be seen that the self-polymerization of dopamine mainly happened on the membrane surface, while the cross section deep inside the membrane was almost not influenced by PDA.[34] Obviously, the MSiM adsorbed more PDA particles than the HM and MSoM. With extending the deposition time from 2 h to 24 h, more polydopamine particles with a size of ~100 nm were

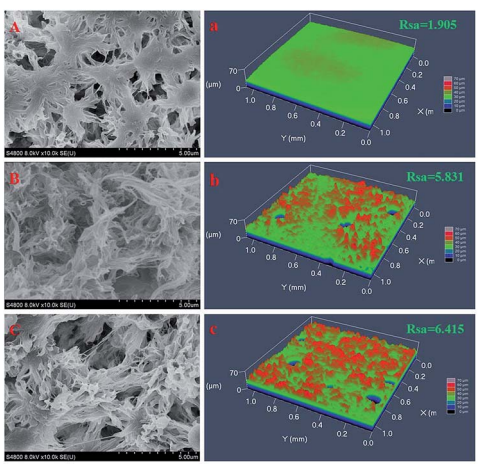

Fig. 4 SEM images with a magnification ×10.0k and confocal roughness of (A), (a) HM, (B), (b) MSiM and (C), (c) MSoM respectively.

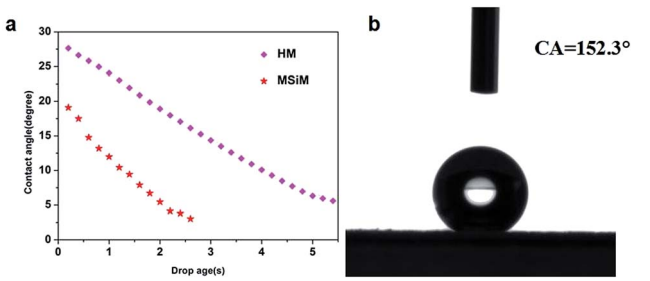

Fig. 5 (a) The contact angle decay of the HM and MSiM with drop age. (b) Static contact angle of the MSoM.

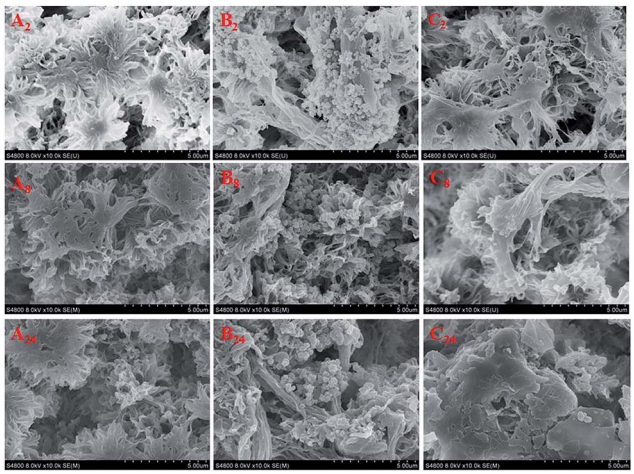

Fig. 6 SEM images with magnification ×10.0k of the PDA–PVDF membranes (A: HM, B: MSiM and C: MSoM) with different PDA deposition times 2 h, 8 h, 24 h.

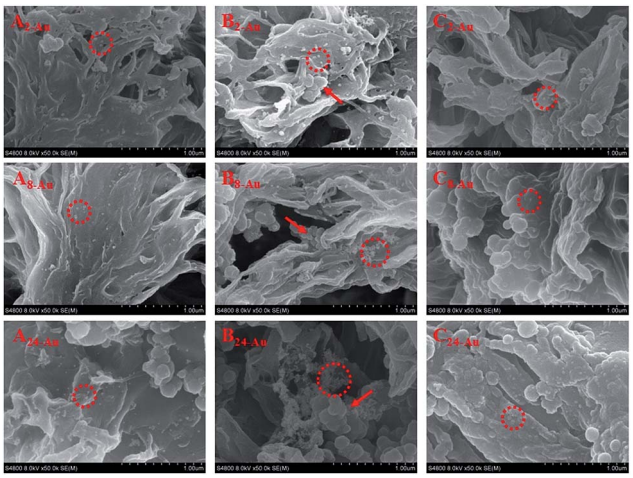

Fig. 7 SEM images with magnification ×50.0k of the Au–PDA–PVDF membranes.

agglomerated and attached to the grooves, fibers, petals and leaves of the membrane surface. Distinctly different from the MSiM, the MSoM adsorbed much less PDA despite the deposition time. Actually, the surface deposition and the self-polymerization in the solution happened competitively.[35–37] The diffusion of hydrophilic dopamine onto the membrane interface is dominating the subsequent surface deposition and growth of the PDA. The MSoM surface repels the diffusion and adsorption of dopamine through the superhydrophobic interactions. Therefore, more PDA tend to be self-polymerized in the solution rather than on the membrane surface. While the superhydrophilic surface favors the diffusion and adsorption of dopamine through hydrophilic interaction. Consequently more PDA was self-polymerized on the membrane surface to form an intermediate bio-glue spacer attributed to amino, imino, hydroxyl and catechol functional group interactions.[38,39] Besides, surface crosslinked PVP segments on the membrane can also form hydrogen bonds with dopamine to promote the adsorption of PDA, which is in accordance with previous studies.[40,41]

The PDA deposited PVDF membrane was capable of capturing AuNPs through the strong adsorption. The Au–PDA–PVDF membrane was therefore produced *via* simple immersion for 24 h. Both the membrane affinity and immersion time will influence the growth and embedding of the AuNPs on the membrane surface. The AuNPs distribution was observed in Fig. 7 with a high magnification of ×50.0k. It can be seen that the $B_{2\text{-Au}}$, $B_{8\text{-Au}}$ and $B_{24\text{-Au}}$ membrane anchored a certain amount of AuNPs with a diameter of ~40 nm, which is circled in the image. PDA particles with a diameter of ~100 nm are identified by a red arrow. $B_{2\text{-Au}}$ showed a quite uniform distribution of AuNPs. However, the agglomeration of AuNPs is getting more serious with extending the deposition time of PDA, demonstrating that higher amounts of AuNPs are embedded onto the MSiM membranes through the bio-glue spacer. Lower amounts of AuNPs are distributed on the $A_{2\text{-Au}}$, $A_{8\text{-Au}}$ and $A_{24\text{-Au}}$ membrane surface without serious agglomeration. The $C_{2\text{-Au}}$, $C_{8\text{-Au}}$ and $C_{24\text{-Au}}$ membrane anchored a lower amount of AuNPs. From the AuNPs distribution on the PVDF membranes with different affinities, we can see that the presence of PDA plays a crucial role for anchoring AuNPs as a bio-glue. It is probably thought that the active –OH groups of PDA are responsible for the assembly of the AuNPs. The hydrophilic surface with the micro/nano structure will promote the deposition of PDA and favor the growth of AuNPs accordingly.[42] Therefore, the superhydrophilic PVDF membrane $B_{2\text{-Au}}$ with the hierarchical surface captured more AuNPs than others. Nevertheless, the intensive agglomeration can decay the membrane catalytic performance. The Au element mass concentration was confirmed using XPS as shown in Table 2. $B_{2\text{-Au}}$ displayed the highest Au content of 5.43%, $A_{2\text{-Au}}$ showed a lower Au loading of 3.33%, and $C_{2\text{-Au}}$ only possessed 0.4% Au. The chemistry composition is well in accordance with the SEM distribution.

3.4 Static catalytic performance of the Au–PDA–PVDF membrane

The remediation of micro-polluted water containing nitrophenols and derivatives is urgent and challenging. The degradation of toxic aromatic phenolic compounds from dyes, herbicides, pesticides and wastewater is difficult to treat *via* the traditional biodegradation methods *e.g.* MBR. Besides, the

Table 2 Element mass concentration using XPS

	XPS mass concentration (%)				
Sample	F	O	N	C	Au
$A_{2\text{-Au}}$	29.01	10.63	3.76	53.26	3.33
$B_{2\text{-Au}}$	26.49	11.33	3.29	53.45	5.43
$C_{2\text{-Au}}$	33.9	11.93	1.88	51.89	0.4

accumulation of the non-degradable compounds on the membrane interface will aggravate the fouling concern. Herein, the reduction of 4-NP to 4-aminophenol (4-AP) using $NaBH_4$ was chosen as the model reaction to evaluate the catalytic performance of the Au–PDA–PVDF membrane. The reduced 4-AP is less toxic and useful in many applications including analgesic and antipyretic drugs, photographic developer, corrosion inhibitor, anticorrosion lubricant, and so on.[43–46] The reduction of 4-NP using $NaBH_4$ in the presence of noble metal nanoparticles has been intensively investigated for the efficient production of 4-AP.[47] Usually versatile AuNPs with different sizes, in the forms of spheres, rods, shells, stars, cages *etc.* are synthesized and directly dispersed in the 4-NP solution for the catalytic reduction. However, the dispersed AuNPs are difficult to recycle and also the catalytic activity will be impaired due to the gradual aggregation. To overcome the deficiency, the AuNPs are therefore firmly anchored and integrated onto a PVDF membrane. Au–PDA–PVDF (MSiM) was immersed in the 4-NP solution instead of freely dispersed AuNPs. The mixtures of 4-NP and $NaBH_4$ show a strong adsorption peak at 400 nm, corresponding to the 4-NP ions under alkaline conditions.[48] After the Au–PDA–PVDF catalytic membrane was added into the mixture, the reduction process was monitored by measuring the time-dependent adsorption spectra. As shown in Fig. 8, the absorption intensity of the 4-NP at 400 nm decreases quickly with time, accompanied by the appearance of the new peaks of 4-AP at 230 nm and 300 nm, indicating the reduction of 4-NP to 4-AP.[49] It is worth noting that the reduction of 4-NP to 4-AP was completely finished in 5 minutes upon the addition of the MSiM $B_{2\text{-}Au}$ as shown in Fig. 8a. The yellow-green color of the pristine aqueous solution undergoes a fading and ultimate bleaching. With increasing the PDA deposition time, the catalytic reduction of 4-NP for $B_{8\text{-}Au}$ and $B_{24\text{-}Au}$ was not further accelerated in Fig. 8b and c. It is speculated that the aggregation has a negative impact on the catalysis. Due to the presence of a large excess of $NaBH_4$ compared to 4-NP, the rate of reduction is independent of the concentration of $NaBiH_4$. The reaction could be considered to be pseudo-first-order with respect to the concentration of 4-NP.[50] Hence, $\ln(C_t/C_0)$ *versus* time can be obtained based on the absorbance as the function of time, and a good linear correlation was observed as shown in Fig. 8d, suggesting that the reduction of 4-NP to 4-AP follows pseudo-first-order kinetics. The kinetic reaction rate constant is calculated from the slope of the linear relationship to be 15.53×10^{-2} min^{-1} (24 h), 42.11×10^{-2} min^{-1} (8 h), 47.84×10^{-2} min^{-1} (2 h). $B_{2\text{-}Au}$ displayed superior catalytic performance to other Au embedded substrates.[51–53] It could be elucidated that the superhydrophilic surface and π–π stacking interactions between the dopamine and 4-NP promoted the initial adsorption, and therefore enhanced the local concentration of 4-NP on the membrane interface. Besides, plenty of confined micropores in the hierarchical membrane surface caged the phenolic compounds. Finally, the well distributed AuNPs on $B_{2\text{-}Au}$ were able to catalyze the reduction reaction efficiently.

In comparison, the HM was also used to catalyze the reduction of 4-NP. It was found that 90% of 4-NP was reduced in ~14 minutes *via* the catalysis of $A_{24\text{-}Au}$ as shown in Fig. 9c. The reaction rate constant of $A_{2\text{-}Au}$, $A_{8\text{-}Au}$ and $A_{24\text{-}Au}$ is 10.44×10^{-2} min^{-1} (2 h), 14.11×10^{-2} min^{-1} (8 h) and 20.43×10^{-2} min^{-2} (24 h) respectively in Fig. 9d. With extending the PDA deposition time, the reduction time was shortened accordingly. It is mainly because the embedding of AuNPs on the HM is far beyond the agglomeration. Therefore, prolonging the deposition time favors the catalytic reduction. The superhydrophobic membrane didn't show any catalytic reduction of 4-NP even in 1 h. The superhydrophobicity of the MSoM makes it difficult to load AuNPs on the MSoM, the poor catalytic performance may be due to the hydrophobicity and the lack of AuNPs on the membrane.

The complexity in separating and recovering the Au nanoparticles from the reaction solution restricted the catalytic stability of the freely dispersed catalysts. The Au–PDA–PVDF membrane eliminated the concerns of catalyst loss and catalytic

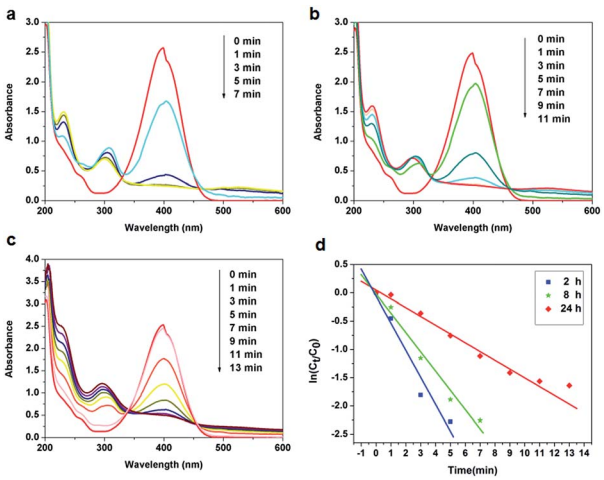

Fig. 8 UV-vis adsorption spectra of the reduction of 4-NP using $NaBH_4$ in the presence of Au–PDA–PVDF (MSiM) (a) $B_{2\text{-}Au}$, (b) $B_{8\text{-}Au}$, (c) $B_{24\text{-}Au}$, (d) plot of $\ln(C_t/C_0)$ of 4-NP *versus* time.

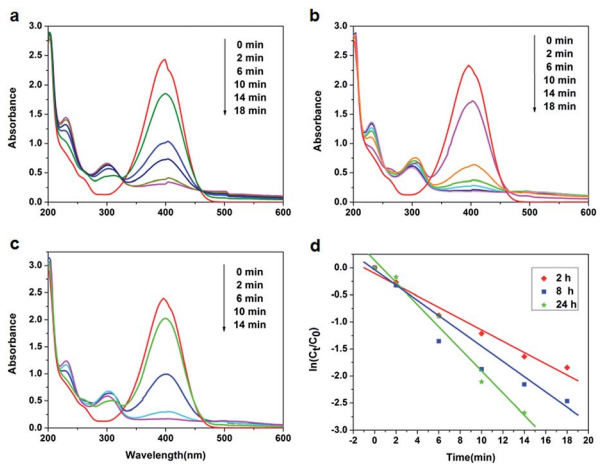

Fig. 9 UV-vis adsorption spectra of the reduction of 4-NP using $NaBH_4$ in the presence of Au–PDA–PVDF (HM) (a) $A_{2\text{-}Au}$, (b) $A_{8\text{-}Au}$, (c) $A_{24\text{-}Au}$ (d), plot of $\ln(C_t/C_0)$ of 4-NP *versus* time.

stability. The MSiM exhibited a good recyclability for the catalytic reduction of 4-NP. It was found that more than 85% of the 4-NP was still reduced to 4-AP in 15 minutes even after 6 cycles as shown in Fig. 10. In contrast, the freely dispersed AuNPs lost the pristine catalytic performance dramatically after reuse due to the severe aggregation of the Au nanoparticles and the loss of catalytic activity. Only 10% of the 4-NP was reduced even in 15 minutes. The results demonstrated that the AuNP modified superhydrophilic PVDF membrane has an excellent catalytic activity and good reusability.

3.5 Membrane catalytic reactor (MCR)

A membrane catalytic reactor (MCR) was designed by sealing a piece of Au–PDA–PVDF membrane ($B_{2\text{-Au}}$, $D = 2.5$ cm) in a cell. The 4-NP aqueous solution was circulated in the MCR using a peristaltic pump with a flow rate of 0.121 mL s^{-1}. The sufficiently high flux is calculated as 887.2 L m^{-2} h^{-1}. The filtrate was collected at different operation durations and analyzed using UV as shown in Fig. 11. With extending the circulation time, the adsorption peak at ~400 nm declined and the peaks at 230 nm and 300 nm grew gradually, indicating the conversion of 4-NP to 4-AP. 90% of the 4-NP was successfully reduced to 4-AP in 30 min. 4-NP was first adsorbed and adhered to the surface of the AuNPs *via* the oxygen atoms of the nitro group and formed an intermediate, which activated the electron transport from the donor BH_4^- ions to the 4-NP. This finally realized the reduction of the nitro group to the amino group.[54,55] From the analysis of the catalytic mechanism, we can see that the resistance time in the MCR influences the contacting of 4-AP with the AuNPs. The kinetic reaction rate constant was determined to be 7×10^{-2} min^{-1} from the slope of the $\ln(C_t/C_0)$ *versus* time plots in Fig. 11. Nevertheless, it is promising to realize the instantaneous catalytic degradation of 4-NP in a flow-through mode when a less porous membrane was applied. Overall, the proof of concept membrane catalytic reactor was successfully verified using the continuous catalytic degradation of 4-NP.

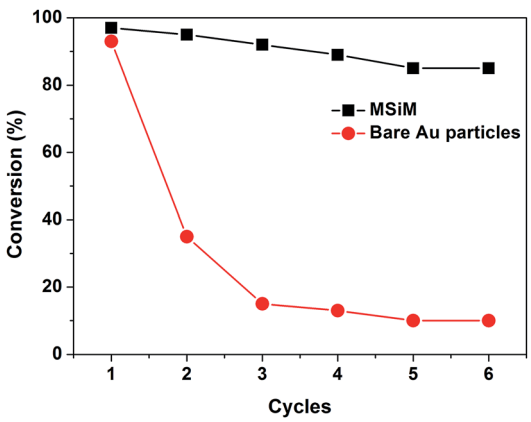

Fig. 10 The stability of the catalytic performance of Au–PDA–PVDF (MSiM) $B_{2\text{-Au}}$ and bare AuNPs in 15 min. Conditions: [4-NP] = 2.72×10^{-5} M, 1.5 mL, [$NaBH_4$] = 0.048 M, 1.5 mL, the area of the membrane is 0.6×0.7 cm^2.

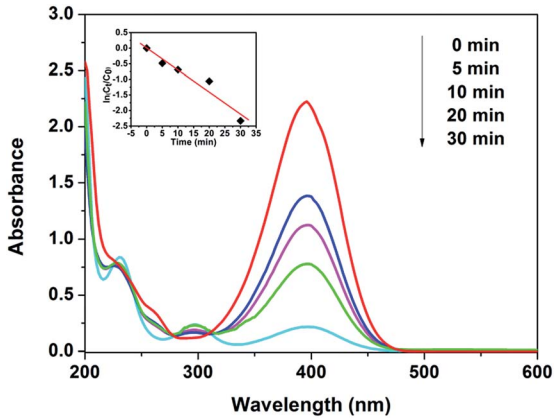

Fig. 11 UV-vis adsorption spectra of the reduction and the plot of $\ln(C_t/C_0)$ of 4-NP *versus* time in the presence of $B_{2\text{-Au}}$.

4. Conclusion

In summary, a catalytic PVDF membrane integrated with AuNPs through PDA as a spacer was successfully prepared for the degradation of 4-NP. The chemical affinity and physical micro/nano structure dominated the deposition of PDA and decoration with the AuNPs, which was confirmed using SEM and XPS. The synergistic effect of superhydrophilicity, hierarchical micropores, and the bio-glue PDA enhanced the adsorption of 4-NP. The well distributed AuNPs on $B_{2\text{-Au}}$ acquired superior catalytic performance. 90% of 4-NP was reduced in 5 minutes, and the kinetic reaction rate constant was 47.84×10^{-2} min^{-1}. Also $B_{2\text{-Au}}$ showed excellent catalytic stability and recyclability. More than 90% of 4-NP was reduced to 4-AP in 30 minutes in a membrane catalytic reactor. The kinetic reaction rate constant is 7×10^{-2} min^{-1}. We show that this approach enables the stable immobilization of nano-catalysts on the surface of a porous membrane. The integrated MCR overcomes the current limitation of a sole filtration membrane or freely dispersed catalysts. The membrane reactor is expected to be valuable to efficiently remove high toxic micro-pollutants *e.g.* aromatic compounds, pesticides, dyes and pharmaceuticals *etc.*

Acknowledgements

This work is financially supported by the National Natural Science Foundation of China (51473177, 51273211), and the Youth Innovation Promotion Association of Chinese Academy of Sciences (2014258).

Notes and references

1 V. Kumar, P. Kumar, A. Nandy and P. P. Kundu, *RSC Adv.*, 2016, **6**, 23571–23580.
2 Y. Zhang and P. Li, *RSC Adv.*, 2015, **5**, 98118–98129.
3 W. Wei, *RSC Adv.*, 2014, **4**, 11159–11167.
4 A. Bottino, G. Capannelli and A. Comite, *Desalination*, 2002, **146**, 35–40.

5 A. Sumisha, G. Arthanareeswaran, A. F. Ismail, D. P. Kumar and M. V. Shankar, *RSC Adv.*, 2015, **5**, 39464–39473.
6 J. Fendler and Y. Tian, *Nanoparticles and Nanostructured Films: Preparation, Characterization and Applications*, 2007, pp. 429–461.
7 R. A. Damodar, S.-J. You and H.-H. Chou, *J. Hazard. Mater.*, 2009, **172**, 1321–1328.
8 D. M. Dotzauer, S. Bhattacharjee, Y. Wen and M. L. Bruening, *Langmuir*, 2009, **25**, 1865–1871.
9 M. Sureshkumar, P.-N. Lee and C.-K. Lee, *J. Mater. Chem.*, 2011, **21**, 12316–12320.
10 A. Piasecka, R. Bernstein, F. Ollevier, F. Meersman, C. Souffreau, R. M. Bilad, K. Cottenie, L. Vanysacker, C. Denis and I. Vankelecom, *Sep. Purif. Technol.*, 2015, **141**, 314–321.
11 N. A. Hashim, Y. Liu and K. Li, *Chem. Eng. Sci.*, 2011, **66**, 1565–1575.
12 M. Buonomenna, P. Macchi, M. Davoli and E. Drioli, *Eur. Polym. J.*, 2007, **43**, 1557–1572.
13 D. Correia, C. Ribeiro, V. Sencadas, G. Botelho, S. Carabineiro, J. G. Ribelles and S. Lanceros-Méndez, *Prog. Org. Coat.*, 2015, **85**, 151–158.
14 S. A. Carabineiro, M. F. Pereira, J. N. Pereira, C. Caparros, V. Sencadas and S. Lanceros-Mendez, *Nanoscale Res. Lett.*, 2011, **6**, 1–5.
15 S. Carabineiro, M. Pereira, J. Nunes-Pereira, J. Silva, C. Caparrós, V. Sencadas and S. Lanceros-Méndez, *J. Mater. Sci.*, 2012, **47**, 8103–8111.
16 S. H. Ku, J. S. Lee and C. B. Park, *Langmuir*, 2010, **26**, 15104–15108.
17 S. H. Ku, J. Ryu, S. K. Hong, H. Lee and C. B. Park, *Biomaterials*, 2010, **31**, 2535–2541.
18 J. Ryu, S. H. Ku, H. Lee and C. B. Park, *Adv. Funct. Mater.*, 2010, **20**, 2132–2139.
19 T. Łuczak, *Electrochim. Acta*, 2008, **53**, 5725–5731.
20 Y. Zhang, H. Wang, J. Nie, H. Zhou, G. Shen and R. Yu, *Electrochem. Commun.*, 2009, **11**, 1936–1939.
21 B. Fei, B. Qian, Z. Yang, R. Wang, W. Liu, C. Mak and J. H. Xin, *Carbon*, 2008, **46**, 1795–1797.
22 H. Hu, B. Yu, Q. Ye, Y. Gu and F. Zhou, *Carbon*, 2010, **48**, 2347–2353.
23 B. D. McCloskey, H. B. Park, H. Ju, B. W. Rowe, D. J. Miller, B. J. Chun, K. Kin and B. D. Freeman, *Polymer*, 2010, **51**, 3472–3485.
24 F. Pan, H. Jia, S. Qiao, Z. Jiang, J. Wang, B. Wang and Y. Zhong, *J. Membr. Sci.*, 2009, **341**, 279–285.
25 H. Lee, S. M. Dellatore, W. M. Miller and P. B. Messersmith, *Science*, 2007, **318**, 426–430.
26 R.-X. Zhang, L. Braeken, P. Luis, X.-L. Wang and B. Van der Bruggen, *J. Membr. Sci.*, 2013, **437**, 179–188.
27 M. Tao, L. Xue, F. Liu and L. Jiang, *Adv. Mater.*, 2014, **26**, 2943–2948.
28 P.-Y. Zhang, H. Yang, Z.-L. Xu, Y.-M. Wei, J.-L. Guo and D.-G. Chen, *J. Polym. Res.*, 2013, **20**, 1–13.
29 I.-S. Cho, J. H. Kim and S. S. Kim, *Korea Polym. J.*, 1997, **5**, 191–198.
30 G. Frens, *Nature*, 1973, **241**, 20–22.
31 W. S. Sutherland and J. D. Winefordner, *J. Colloid Interface Sci.*, 1992, **148**, 129–141.
32 J. Li, C.-Y. Liu and Y. Liu, *J. Mater. Chem.*, 2012, **22**, 8426–8430.
33 Y. Zhang, S. Liu, W. Lu, L. Wang, J. Tian and X. Sun, *Catal. Sci. Technol.*, 2011, **1**, 1142–1144.
34 Y. Xiang, F. Liu and L. Xue, *J. Membr. Sci.*, 2015, **476**, 321–329.
35 F. Bernsmann, V. Ball, F. Addiego, A. Ponche, M. Michel, J. J. A. Gracio, V. Toniazzo and D. Ruch, *Langmuir*, 2011, **27**, 2819–2825.
36 N. F. Della Vecchia, R. Avolio, M. Alfè, M. E. Errico, A. Napolitano and M. d'Ischia, *Adv. Funct. Mater.*, 2013, **23**, 1331–1340.
37 F. Bernsmann, A. Ponche, C. Ringwald, J. Hemmerlé, J. Raya, B. Bechinger, J.-C. Voegel, P. Schaaf and V. Ball, *J. Phys. Chem. C*, 2009, **113**, 8234–8242.
38 Z. Iqbal, E. P. Lai and T. J. Avis, *J. Mater. Chem.*, 2012, **22**, 21608–21612.
39 P. Henke, H. Kozak, A. Artemenko, P. Kubát, J. Forstová and J. Mosinger, *ACS Appl. Mater. Interfaces*, 2014, **6**, 13007–13014.
40 Y. Zhang, B. Thingholm, K. N. Goldie, R. Ogaki and B. Städler, *Langmuir*, 2012, **28**, 17585–17592.
41 Q. Zhu and Q. Pan, *ACS Nano*, 2014, **8**, 1402–1409.
42 J. Jiang, L. Zhu, L. Zhu, B. Zhu and Y. Xu, *Langmuir*, 2011, **27**, 14180–14187.
43 Y. Du, H. Chen, R. Chen and N. Xu, *Appl. Catal., A*, 2004, **277**, 259–264.
44 J. F. Corbett, *Dyes Pigm.*, 1999, **41**, 127–136.
45 C. Rode, M. Vaidya and R. Chaudhari, *Org. Process Res. Dev.*, 1999, **3**, 465–470.
46 Z. Zhang, C. Shao, P. Zou, P. Zhang, M. Zhang, J. Mu, Z. Guo, X. Li, C. Wang and Y. Liu, *Chem. Commun.*, 2011, **47**, 3906–3908.
47 Y. Deng, Y. Cai, Z. Sun, J. Liu, C. Liu, J. Wei, W. Li, C. Liu, Y. Wang and D. Zhao, *J. Am. Chem. Soc.*, 2010, **132**, 8466–8473.
48 S. Praharaj, S. Nath, S. K. Ghosh, S. Kundu and T. Pal, *Langmuir*, 2004, **20**, 9889–9892.
49 S. Tang, S. Vongehr and X. Meng, *J. Phys. Chem. C*, 2009, **114**, 977–982.
50 J. Huang, S. Vongehr, S. Tang, H. Lu and X. Meng, *J. Phys. Chem. C*, 2010, **114**, 15005–15010.
51 H. Koga, E. Tokunaga, M. Hidaka, Y. Umemura, T. Saito, A. Isogai and T. Kitaoka, *Chem. Commun.*, 2010, **46**, 8567–8569.
52 S. Tang, S. Vongehr and X. Meng, *J. Mater. Chem.*, 2010, **20**, 5436–5445.
53 K. Kuroda, T. Ishida and M. Haruta, *J. Mol. Catal. A: Chem.*, 2009, **298**, 7–11.
54 S. Wunder, F. Polzer, Y. Lu, Y. Mei and M. Ballauff, *J. Phys. Chem. C*, 2010, **114**, 8814–8820.
55 Y.-C. Chang and D.-H. Chen, *J. Hazard. Mater.*, 2009, **165**, 664–669.